Clays and Clay Minerals, Vol. 48, No. 5, 511–520, 2000.

FORMATION OF BANDED IRON-MANGANESE STRUCTURES BY NATURAL MICROBIAL COMMUNITIES

KAZUE TAZAKI

Department of Earth Sciences, Faculty of Science, Kanazawa University, Kanazawa, Ishikawa 920-1192, Japan

Abstract—Microbial structures in the form of banded zebra patterns have been found as periodic iron-manganese layers in living biomats on the coast of Satsuma-Iwo Jima, a small volcanic island near southern Kyushu, Japan. Electron microscopic observation shows that coccus, fibrous, and bacillus-type bacterial communities construct zebra architecture Fe-Mn layers through biomineralization on and within cells. A living microbial fumarolic ferro-manganese precipitation growing in seawater around an active volcanic island explains one mechanism of banded formation. Biological processes form the elemental zebra pattern, with periodic distribution of bacterial cells with Fe-Mn in each layer of the architecture. Fibrous bacteria are sometimes mineralized with goethite, ferrihydrite, and buserite microcrystals, coated with granular mucoid substances. The biomineralization may then mature to form a recent stratified banded-iron formation. The Satsuma-Iwo Jima zebra architecture is unusual in that it forms under aerobic conditions in a warm shallow-water environment, in contrast to the intermittent oxidizing and reducing conditions in which deep-sea analogues develop.

Key Words—Bacteria, Banded Fe-Mn Structure, Biomats, Biomineralization, Zebra Architecture.

INTRODUCTION

Microbial metabolic reactions can have widespread influence on the geochemistry of natural waters through oxidation and reduction of iron and other inorganic ions. The terrestrial surface and subsurface waters are sites of geochemical cycling in the natural environment, but it has only recently been recognized that these reactions are generally mediated by the activity of microorganisms, usually bacteria (Brown *et al.,* 1999). Such reactions and geochemical cycling are also important in the genesis of ore deposits. Biomineralogical and geochemical studies of iron and manganese precipitation in recent lakes, the deep sea, and brines have promoted the understanding of the processes responsible for formation of fossil iron and manganese deposits (Frankel and Blakemore, 1991; Skinner and Fitzpatrick, 1992; Brown *et al.,* 1998; Tazaki, 1999).

Widespread bacterial fixation of metallic ions contributes to immobilization of mineral-forming elements through a continuum of reactions involving sorption and authigenic mineral precipitation (Ferris *et al.,* 1987; Emerson and Revsbech, 1994; Tazaki, 1997; Tazaki *et al.,* 1998). Holden (1998) reported ancient zebra patterns in a 30 million year old limestone from Germany, and stated that inorganic processes could produce the magnificent patterns observed. However, bacterial activity may also be suspected, even in this earliest example of zebra-pattern formation. Occurrence of voluminous Archean-Proterozoic Fe-rich beds in the form of banded-iron formations (BIF) demonstrates the important role of bacterial biomineralization in the early stages of Earth history.

Recent studies show that living biofilms contain variable distributions of heavy metal elements in their cells and cellular aggregates, in their extracellular polymers, and in void spaces or water channels which may or may not be connected with ambient liquid phases. This paper reports and discusses recent banded iron-manganese structures formed by natural microbial communities around the small active volcanic island Satsuma-Iwo Jima (Sulfur Island), located 50 km south of Satsuma Peninsula, Kagoshima, southern Kyushu, Japan.

Satsuma-Iwo Jima is an active volcanic island comprising a basalt volcano and a rhyolite somma dome built on the margin of Kikai Caldera, which erupted 6000 years ago (Figure 1). Numerous active hot springs occur on and around the island. Colorful biomats can be seen in hot springs and geothermal areas. The biomineral assemblages can include carbonates, silicates, hydrated phosphates, sulfides, and clay minerals formed through bacterial activities. The nature of the assemblage is dependent on temperature, pH, Eh, dissolved oxygen (DO), and electrical-conductivity (EC) conditions (Tazaki *et al.,* 1998).

This study examines the coastal occurrences at Akayu Hot Springs and Nagahama Port (Figure 1). The surface seawater of the inlets at both localities is colored reddish-brown by jets of smoky emanations from fumaroles debouching from the inlet floors (Figure 2A).

At Akayu Hot Springs, reddish-brown precipitates derived from the hot springs occur on sand and rock beaches (Figure 2B). These deposits and the reddish-stained seawater give the area its name, "Akayu" (derived from the Japanese "aka", meaning red). Basalt outcropping at Akayu was erupted from the foothills of the Mt. Inamura Dake volcano (Figure 1) in the Holocene (Ono *et al.,* 1982). Reddish-brown biomats

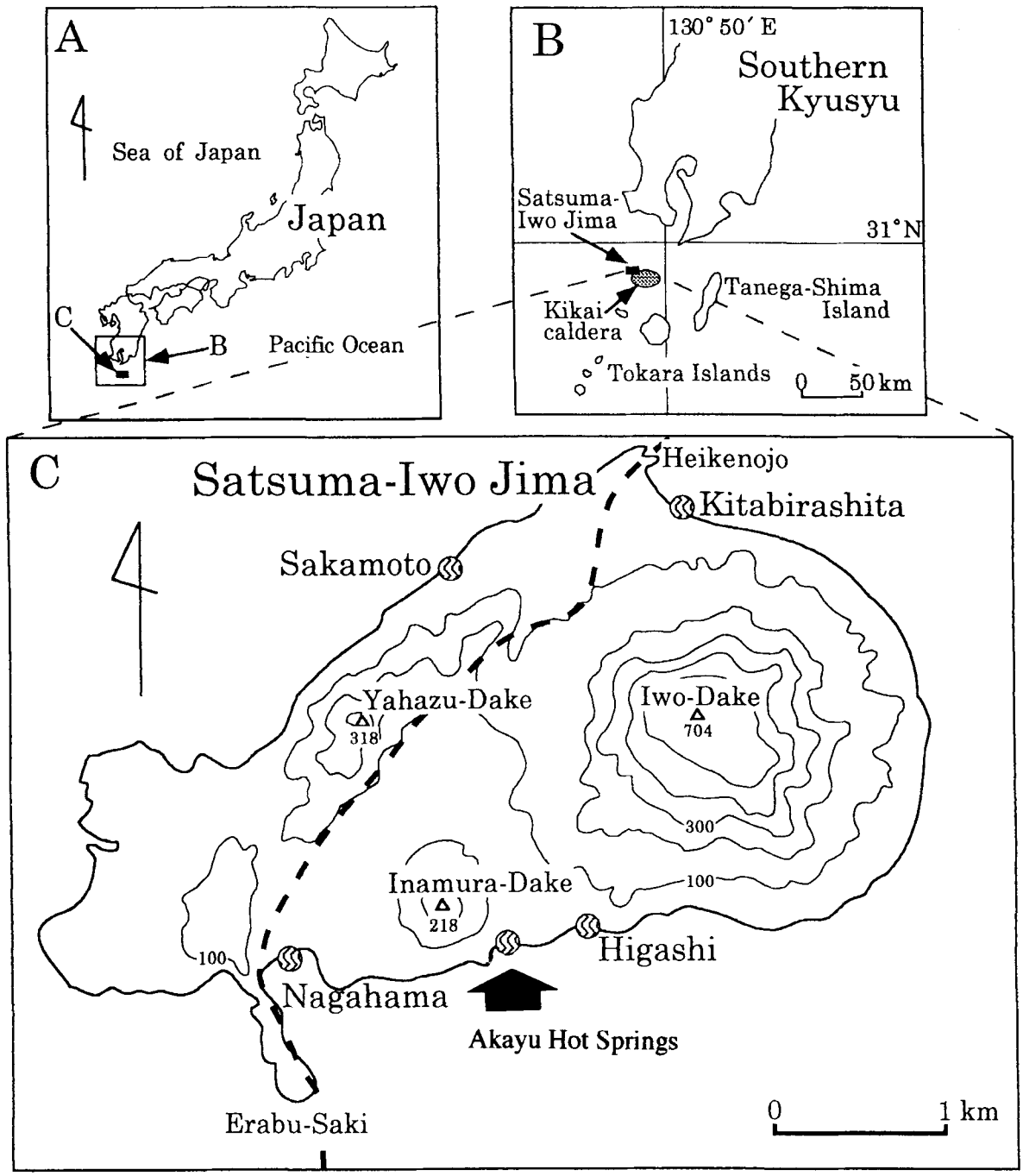

Figure 1. Index maps: (A) Japan showing the location of southern Kyushu. (B) Southern Kyushu showing location of Satsuma-Iwo Jima and Kikai Caldera. (C) Map of Satsuma-Iwo Jima showing the location of Akayu Hot Springs, Nagahama, and other hot spring occurrences. Heavy dashed line is the margin of Kikai Caldera.

with gels and soft materials fill vesicles in porous basalt on the beach. Banded growth ring-like layers are actively growing within the vesicles (Figure 2B). Colloidal material or gels in the reddish-brown biomats gradually hardens into striped structures. Soft and muddy reddish-brown zebra architecture also covers porous basalt surfaces.

Samples were collected from the soft (gel-like) reddish-brown living biomats and hard banded growth ring-like crusts from the rock beach at Akayu Hot

https://doi.org/10.1346/CCMN.2000.0480503 Published online by Cambridge University Press

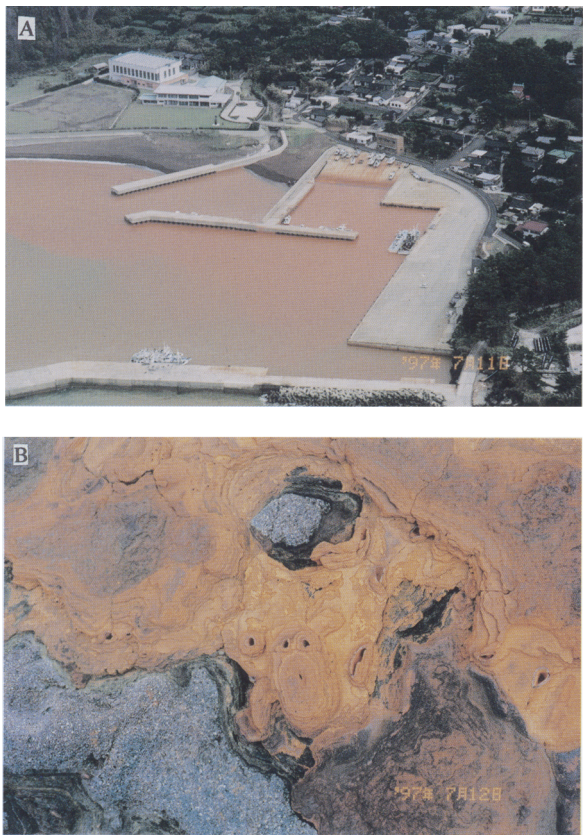

Figure 2. Nagahama port and occurrence of living zebra architecture at Akayu Hot Springs, Satsuma-Iwo Jima. (A) The hot spring water in and around Nagahama port reacts with seawater to produce ferrian manganese sediments. Reddish-brown terrace-like sediments are exposed near the breakwaters at Nagahama at low tide. (B) Reddish-brown zebra architecture formed on basalt at Akayu Hot Springs.

Springs. The reddish seawater was also sampled to examine living microorganisms. Samples of varying shades of colored seawater were also taken for water chemistry analysis. Temperature (WT), pH, Eh, EC, and DO differ in each seawater sample (Table 1). Water temperatures were relatively high (24.9–26.4°C), and low pH was characteristic for these waters.

Table 1. Water chemistry of colored sea water at Akayu Hot Springs.

Samples	pH	[1]EC (ms/cm)	Eh (mV)	[2]DO (mg/L)	[3]WT (°C)
Reddish	3.12	48	440	8.14	26.4
Brown	4.66	49	230	7.42	25.8
Ivory	5.45	50	166	7.79	25.0
Reddish	7.29	45	180	7.81	24.9
Reddish	6.20	48	439	6.76	24.9

[1] Electrical conductivity.
[2] Dissolved oxygen.
[3] Water temperature.

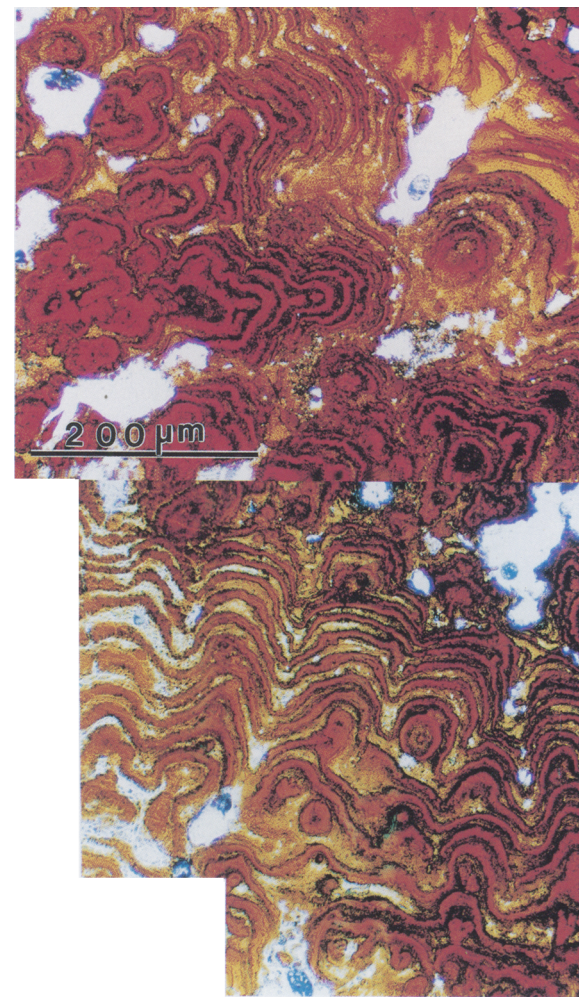

Figure 3. Optical micrograph of a thin section of the hardened periodic zebra-architecture precipitate at Akayu Hot Springs, showing reddish-brown and black banded layers.

MATERIALS AND METHODS

Shoreline hot-water pools are repeatedly replenished by seawater. Reddish seawater and smear slides of the soft and muddy reddish-brown biomats were examined under a polarizing optical and fluorescent microscope (Nikon EFD3) using acridine orange and 4,6-diamidino-2-phenylindole (DAPI) staining. Polished thin sections of hard banded crust samples were examined by electron probe microanalysis (EPMA) with a JEOL JXA8800R Super Probe at an accelerating voltage of 15 kV. A Nikon NTF2A optical microscope was used for observation of reddish seawater and gel materials. Both soft and hard samples were also investigated using a JEOL-JSM-5200LV scanning electron microscope (SEM), equipped with an energy dispersive X-ray spectrometer (EDX; Philips-EDAX PV9800STD), and with a JEOL JEM 2000EX transmission electron microscope (TEM).

https://doi.org/10.1346/CCMN.2000.0480503 Published online by Cambridge University Press

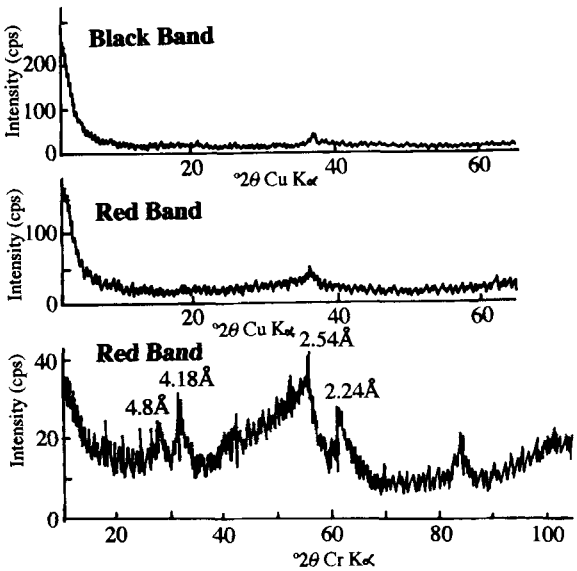

Figure 4. X-ray powder diffraction of hardened biomats showing the amorphous nature of materials in both the black and red bands when using CuKα radiation. CrKα radiation shows that ferrihydrite (2.54 and 2.24 Å) and goethite (4.80, 4.18, and 2.24 Å) coexist with amorphous materials in the red bands.

Mineralogical investigations of oriented clay-aggregate samples were performed by X-ray diffraction (XRD) with a Rigaku Rinto 1200 X-ray diffractometer using CuKα and CrKα radiation. Carbon, sulfur, and nitrogen contents of both soft, muddy living biomats and hard, solidified biomats were also determined using an automatic gas chromatographic elemental analyzer (CE Instruments NA2500-NCS) at 1000°C with 20 mL oxygen. Chemical compositions of the biomats were also determined by energy dispersive X-ray fluorescence analysis (XRF) using a JEOL JSX-3201 instrument.

RESULTS

Optical and fluorescent microscopic observation of reddish seawater and smear slides of the soft and muddy biomats revealed the presence of abundant cocci bacteria (1–5 μm in size) and filamentous bacteria (3–10 μm). Acridine orange and DAPI staining under fluorescent microscopy established that both types of bacteria contained chlorophyll.

Thin-section examination showed that the zebra architecture had a banded structure consisting of alternating micron-sized reddish-brown and black layers (Figure 3). EPMA examination (see below) showed that the reddish-brown layers were rich in iron, and the black layers were rich in manganese. Abundant bacterial colonies were observed at the margin of each band. In the reddish-brown layers, filamentous bacteria were associated with accumulations of a granular iron-bearing phase. Cocci and bacillus bacteria in the black layers concentrated both granular iron and flaky manganese oxides in or on the living cells.

Table 2. Nitrogen, carbon, and sulfur elemental analyses of biomats at Akayu Hot Springs.

Samples	N (wt. %)	C (wt. %)	S (wt. %)	
Surface gel	0.245	3.435	0.400	0 cm
	0.243	3.411	0.408	
	0.246	3.375	0.409	
Ave.	0.245	3.407	0.406	
Zone 1	0.021	0.426	0.182	3 cm
	0.020	0.436	0.173	
	0.020	0.435	0.162	
Ave.	0.020	0.432	0.172	
Zone 2	0.007	0.294	0.207	6 cm
	0.007	0.290	0.204	
	0.006	0.286	0.192	
Ave.	0.007	0.290	0.202	
Zone 3	0.006	0.297	0.224	10 cm
(hardened biomat)	0.006	0.292	0.208	
	0.006	0.293	0.213	
Ave.	0.006	0.294	0.215	

X-ray diffraction analysis of the reddish-brown and black bands exhibited no distinctive diffraction peaks when CuKα radiation was used. However, CrKα radiation showed that ferrihydrite (2.54 and 2.24 Å) and goethite (4.80, 4.18, and 2.24 Å) coexisted with amorphous materials in the reddish-brown bands (Figure 4).

SEM observation showed that gel-like, reddish-brown soft tissue was filled with granular bacteria. EDX analysis established that the granular material adhering to the surfaces of cocci and filamentous bacteria colonies contained abundant iron and manganese, derived from seawater (Figure 5).

Gas-chromatography analyses for C, H, and N were made of surface gel and three zones of an underlying 10-cm thick hardened biomat. The results show that C contents decrease from 3.4 wt. % at the surface to 0.4 and 0.3 wt. % in the hardened biomats beneath (Table 2). Nitrogen and sulfur contents also decrease downward, from 0.4 to 0.2 wt. %, and from 0.2 to 0.02 wt. %, respectively. These results clearly show that organic elements such as carbon, sulfur, and nitrogen decrease immediately after death of the organism.

Table 3. Energy dispersive XRF analysis of biomats at Akayu Hot Springs.

Oxide	wt. %	Oxide	wt. %
Na_2O	3.41	K_2O	0.20
MgO	2.66	CaO	1.19
Al_2O_3	3.48	MnO	3.13
SiO_2	7.66	Fe_2O_3	72.90
P_2O_5	0.14	ZnO	0.08
SO_3	1.22	As_2O_3	0.10
Cl	3.76	SrO	0.06

https://doi.org/10.1346/CCMN.2000.0480503 Published online by Cambridge University Press

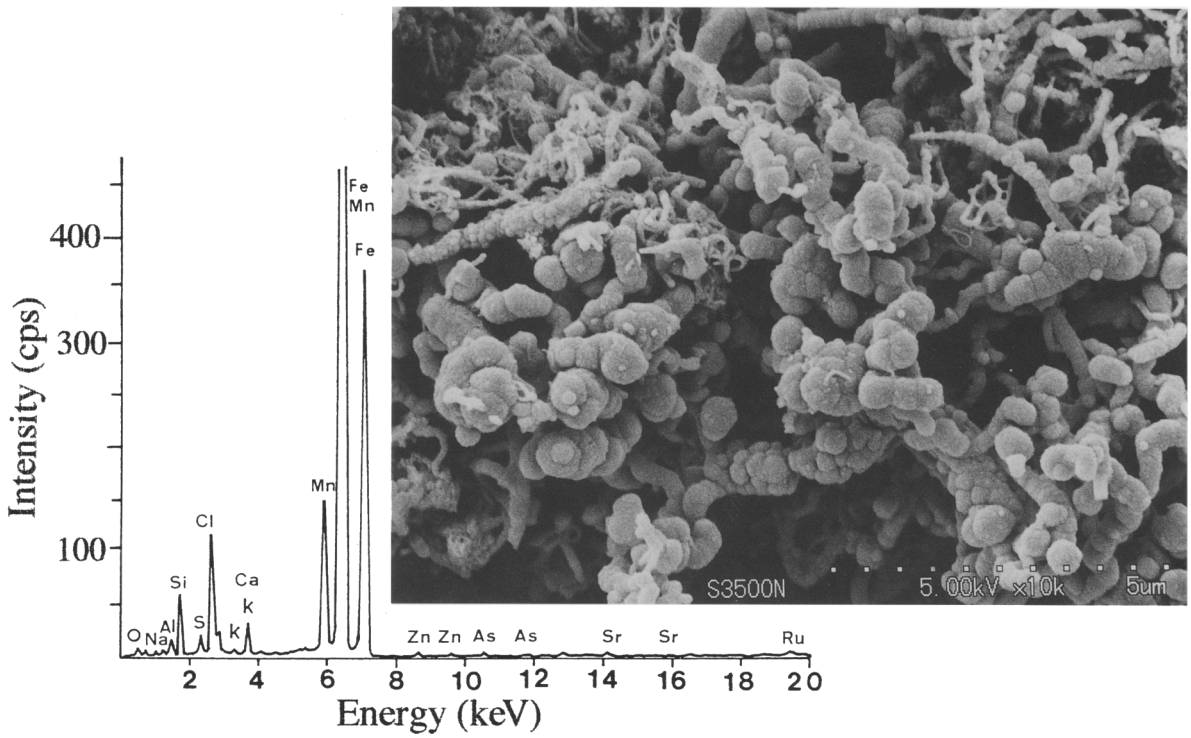

Figure 5. Scanning electron micrograph of gel-like reddish-brown soft tissue showing cocci and filamentous bacterial colonies covered with granular iron and manganese, as identified by energy dispersive X-ray analysis.

XRF analysis of living reddish-brown material collected from a porous basal surface at Akayu Hot Springs is given in Table 3. The bulk biomat sample contains 72.9 wt. % Fe_2O_3T (total iron as ferric iron oxide) and 3.13 wt. % MnO. The minor phosphorous content (0.14 wt. %) suggests the presence of organic materials. Traces of other oxides were found also.

EPMA shows clear compositional banding of zebra architecture, with periodic alternations of iron-rich and manganese-rich layers in rhythms to 50 μm wide (Figure 6). Elemental-content maps show the presence of other elements such as phosphate, sulfur, calcium, and strontium in both the Fe- and Mn-rich layers. Magnesium, however, is associated only with Mn-rich layers, which correspond with the darker parts of the compositional map (CP) (Figure 6, upper left). In some parts, nearly equivalent contents of iron and manganese are observed over widths of 50 μm (Figure 7).

Quantitative analyses produce a profile of elemental concentrations in the bright Fe-rich and dark Mn-rich parts (Figures 6–9). The seven elements analyzed (Table 4) total to 35–52 wt. % in the Mn-rich part (D1 to D7), and to 78–86 wt. % in the Fe-rich section (B1 to B5). The low-oxide sums reflect the presence of large amounts of hydroxides and water, especially in the Mn-rich parts (Table 4).

Total iron as FeO ranges from 45.9–68.3 wt. % in the Fe-rich part to 6.7–20.3 wt. % in the Mn-rich part (Figure 8). Silica contents are also higher in the Fe-rich band (>13 wt. %) than in the Mn-rich part (generally <4 wt. %). Manganese oxides show the reverse

Table 4. Electron microprobe analyses (wt. %) of bright (B) and dark (D) bands of biomats at Akayu Hot Springs.

	B1	B2	B3	B4	B5	D1	D2	D3	D4	D5	D6	D7
SiO_2	12.80	11.07	11.37	11.38	8.45	3.59	2.65	4.13	3.49	2.84	1.99	1.19
Al_2O_3	1.14	1.22	1.52	1.87	2.96	2.84	2.94	2.46	3.03	4.30	3.42	4.37
FeO	68.26	62.14	61.37	62.45	45.89	20.34	10.38	23.14	15.98	14.45	10.55	6.75
MnO	0.56	0.62	1.99	4.00	7.41	15.19	18.32	16.4	19.99	17.62	15.11	14.67
MgO	1.17	1.35	2.04	2.57	5.20	4.96	5.25	4.63	5.61	7.47	6.08	7.52
CaO	1.91	1.56	1.55	1.44	1.11	0.86	0.99	1.19	1.06	0.81	0.64	0.50
Na_2O	0.18	0.23	0.22	0.12	0.17	0.08	0.05	0.09	0.08	0.06	0.06	0.05
Total	86.01	78.2	80.05	83.83	71.19	47.85	40.58	52.03	49.23	47.56	37.85	35.04

https://doi.org/10.1346/CCMN.2000.0480503 Published online by Cambridge University Press

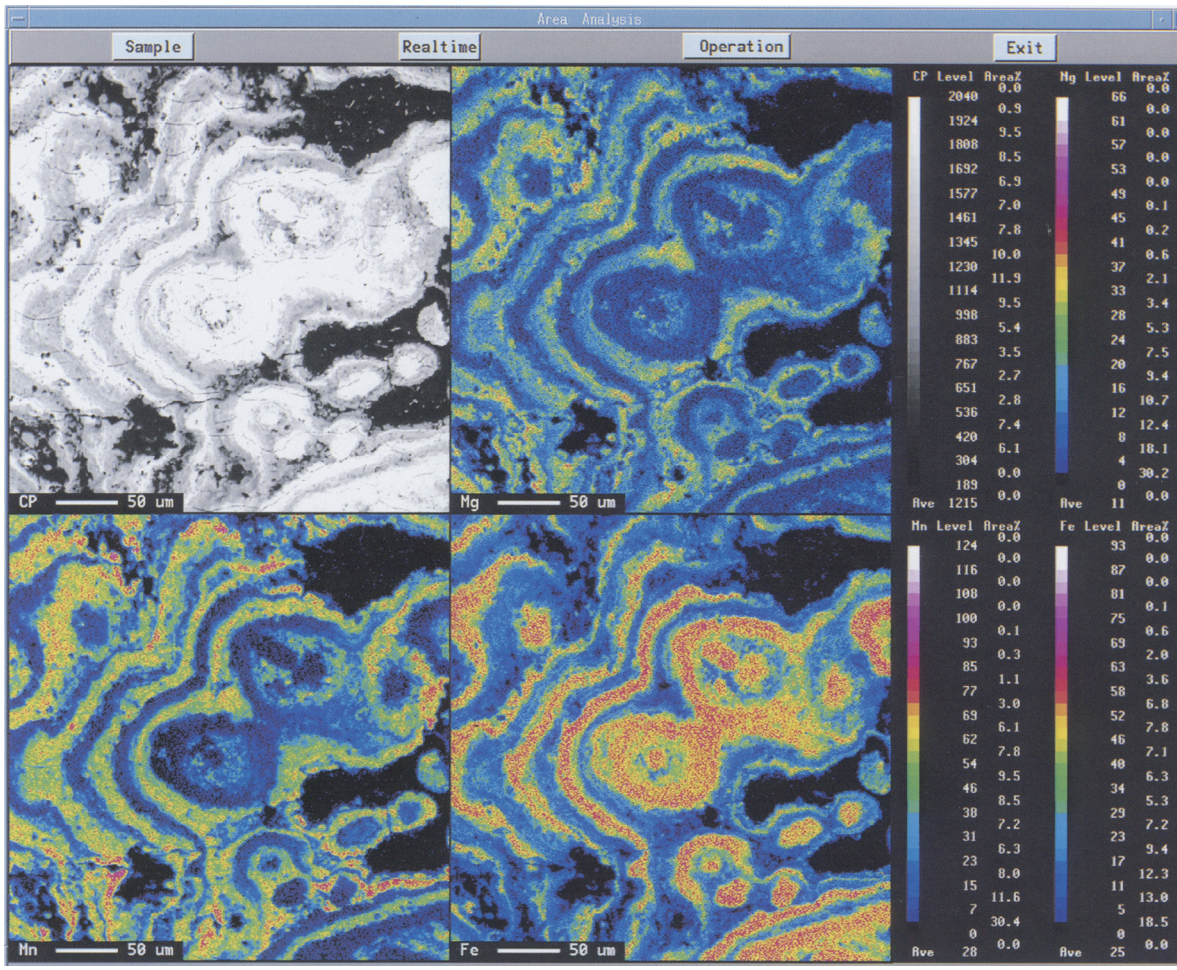

Figure 6. Elemental color maps showing distribution of Mg (upper right), Mn (lower left), and Fe (lower right) in zebra architecture, and a compositional map (CP; upper left). The maps show that precipitation in each ring began with iron. Manganese and associated magnesium was precipitated subsequently. Iron under near neutral pH condition may also have occurred.

pattern, with enrichment (to 20 wt. %) in the dark band, compared to 1.1–7.4 wt. % (generally <2 wt. %) in the bright Fe-rich band. This is also the case for MgO, with contents varying from 6 wt. % (Mn-rich) compared to <2 wt. % (Fe-rich). Al_2O_3 content also increases slightly in the Mn-rich part (Table 4; Figure 8). Representative sequential analyses across a biomat from core to rim (Table 5) also exhibit the elemental distributions and associations noted above (Figures 8 and 9). Iron is associated with silicon, whereas manganese is associated with magnesium (Figure 9).

TEM observations of both reddish-brown and dark tissue confirm the presence of coccus, bacillus, and fibrous bacteria covered with granular iron oxides

Table 5. Electron microprobe analyses (wt. %) from core (1) to rim (9) of a biomat at Akayu Hot Springs.

	1	2	3	4	5	6	7	8	9
SiO_2	10.62	13.36	3.30	13.39	6.08	12.22	2.73	11.12	1.31
Al_2O_3	1.75	1.07	3.69	1.15	3.42	1.11	2.10	1.31	3.48
FeO	61.73	69.46	16.10	68.00	31.29	67.29	14.66	61.80	7.61
MnO	0.86	0.27	16.35	0.38	11.83	0.45	10.05	1.96	17.28
MgO	1.92	1.02	6.20	1.00	5.38	1.07	3.59	1.17	6.09
CaO	1.19	2.09	0.80	1.99	0.81	1.83	0.51	1.51	0.70
Na_2O	0.15	0.18	0.10	0.17	0.08	0.20	0.04	0.16	0.13
Total	78.24	87.44	46.54	86.07	58.89	84.17	33.68	79.04	36.59

https://doi.org/10.1346/CCMN.2000.0480503 Published online by Cambridge University Press

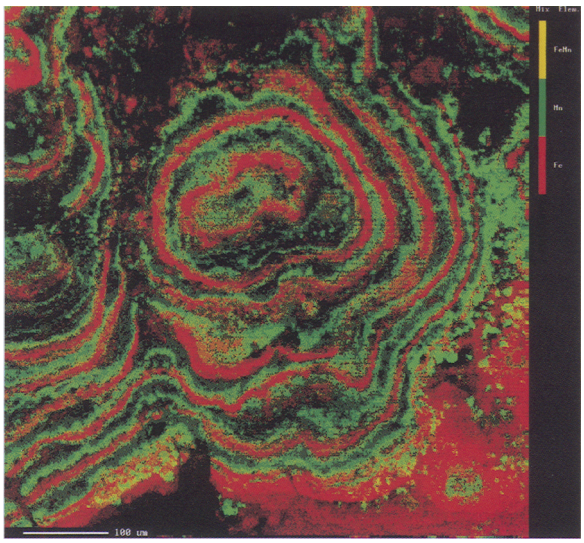

Figure 7. Elemental color map of Fe (red), Mn (green), and Fe + Mn (yellow) in zebra architecture, showing nearly equivalent contents.

(Figure 10) and flaky manganese oxides (Figure 11). Fibrous bacteria in a reddish-brown Fe-rich band were covered with semi-granular materials (Figure 10A and 10B) and bundles of spiny minerals (Figure 10C and 10D).

Some layers exhibit high electron density, indicating that the bacteria were mineralized both inside and outside of the cell wall (Figure 10). X-ray diffraction and EPMA analysis showed that these mineralized parts consist mostly of fine ferrian hydroxide crystals. Well-crystallized spinal minerals around the fibrous bacteria exhibit the 0.5-nm lattice image of goethite (Figure 10C and 10D). Coccus bacteria from a dark Mn-rich band contain fine, coherent, dark materials along their cell walls, and low-density cubic minerals have crystallized inside cells or extend from the cell walls (Figure 11A). These cubic minerals may be halites. Fine spiny and flaky manganese oxides enclose bacillus bacterial cells, and also fill interiors (Figure 11B). High electron densities suggest that the bacteria are covered with long bundles of hair-like manganese oxides (Figure 11C). From the morphology, the flake-like and hair-like manganese oxides are assumed to be buserite. Occurrence of flake-like buserite in biomats was previously produced experimentally (Mandernack *et al.*, 1995; Yoshizu and Tazaki, 1997).

DISCUSSION

Precipitates of iron and manganese forming periodic structures on the beach of Satuma-Iwo Jima Island essentially result from bacterial activity, despite the close association with active submarine fumaroles. Observations of the recent banded iron-manganese structure described here suggest that iron and manganese bacteria produce structures by periodic precipitation (Figures 6–11). The specially defined pattern of these elements has been termed biofilm "architecture"

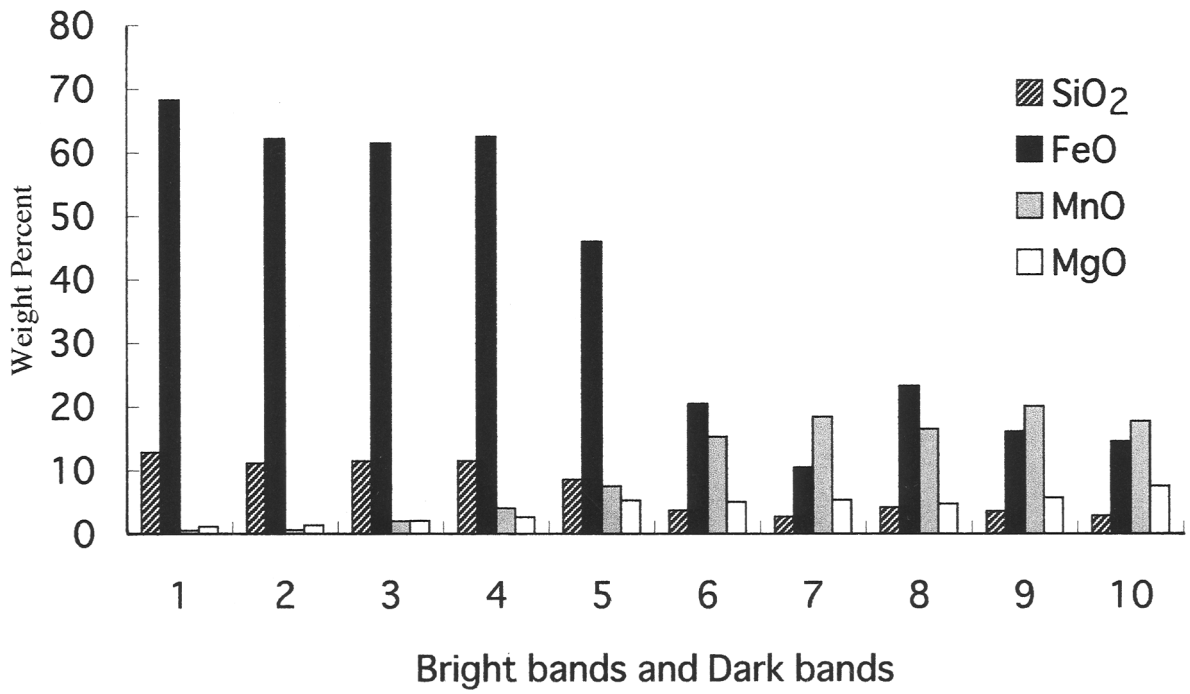

Figure 8. Bar graphs of the four main constituent elements in a thin-sectioned biomat. Analysis points 1 to 5 are in a bright Fe-rich band; points 6 to 10 are in a dark Mn-rich band.

https://doi.org/10.1346/CCMN.2000.0480503 Published online by Cambridge University Press

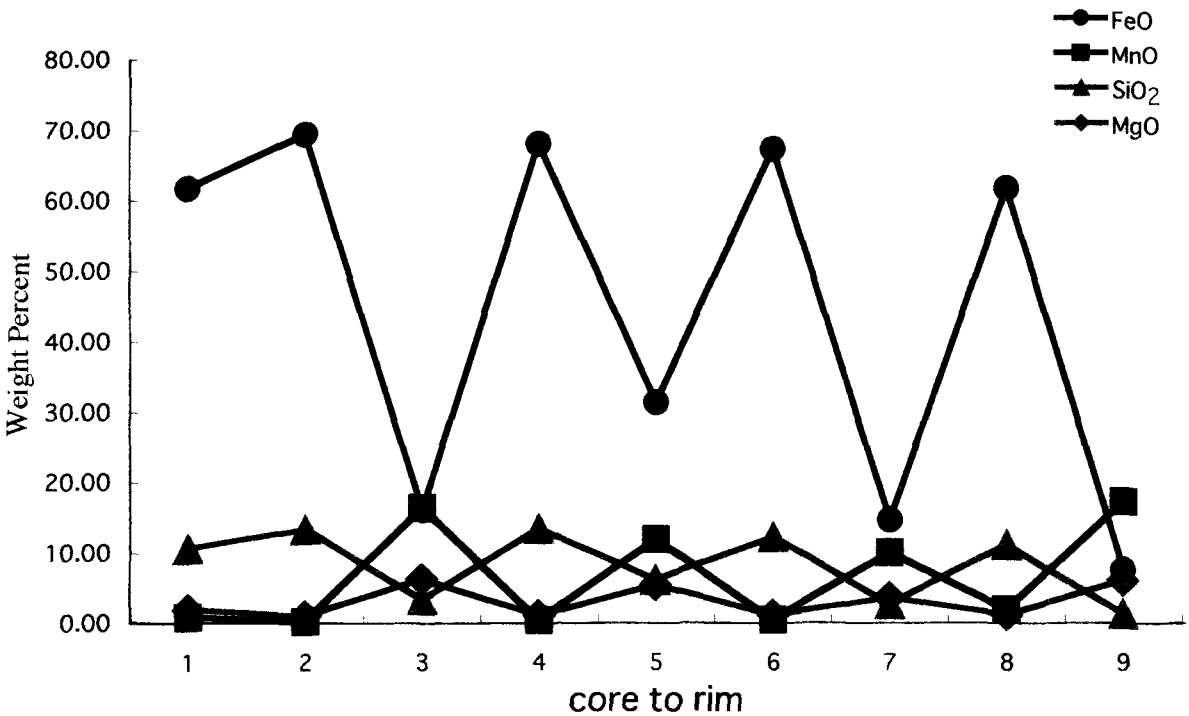

Figure 9. Quantitative electron microprobe analyses of a thin-sectioned biomat from core to rim, showing periodic Fe and Mn distribution in bands.

(Lawrence *et al.,* 1991). Various bacteria, including coccus, bacillus, and fibrous forms, concentrate iron and manganese hydroxides on their cell walls during their lives, and accumulate additional hydroxides on and within cells to form structurally amorphous or crystalline biominerals.

As shown in Figures 5 and 6, iron initially precipitated at the cores of compositional rings, followed by manganese accompanied with magnesium. The EPMA maps and electron micrographs of gel-like reddish-brown soft tissue suggest that iron-oxidizing bacteria grew rapidly and accumulated from acidic seawater at the initial stages of the microbial process. At low pH, such as in the reddish or brown seawaters of Satsuma-Iwo Jima (Table 1), abundant cocci bacteria and filamentous bacteria may grow rapidly, using ferrous ions as their energy source. Other acidophile bacteria can also oxidize ferrous iron enzymatically. Growth of iron-oxidizing bacterial colonies will tend to decrease the acidity of ambient seawater. At near neutral pH, reactions promoted by photosynthetic bacteria produce solid forms of ferric iron such as ferihydrite (Nealson and Stahl, 1997).

Accumulation of removed manganese Mn(II) ions neighboring iron-enriched zones under near neutral seawater conditions provides favorable nutrients for manganese-oxidizing bacteria. Direct microbial oxidation of Mn(II) to Mn(IV) occurs through binding of Mn(II) ions to cell macromolecules such as protein, cell-wall components, and extracellular polymers, with concomitant oxidation (Tebo *et al.,* 1997). Alternate microbial precipitation of iron hydroxides and manganese oxides may proceed with such a two-step process. The banded zebra architecture of iron and manganese in Satsuma-Iwo Jima may however result from a composite process combining biogeochemical factors, tidal influence, and the substrate conditions offered by the rough surface of the porous rock beach.

The earliest stages of biofilm formation are matrix-enclosed bacterial populations adhering to each other and/or to surfaces or interfaces within the pore spaces of the porous media (Lawrence *et al.,* 1991; Costerton *et al.,* 1995). Mucoid substances (polysaccharides) produced by iron bacteria may promote adhesion of iron hydroxides. This results in condensation of iron hydroxides as colloidal particles coated with granular mucoid substances. The rough and porous surface of the basalt on the rock beach at Satsuma-Iwo Jima Provides relief favorable for biomat formation.

Formation of periodic alternations of iron, manganese, and silica-rich strata are well known from the Archean, as represented by BIF (Reitner and Neuweiler, 1995). Iron and manganese oxides occur on the modern seafloor as nodules, ferro-manganese crusts, and metalliferous sediments in settings removed from obvious hydrothermal output, and also as low-temperature hydrothermal mounds and chimneys in close proximity to active vents (Hannington and Jonasson,

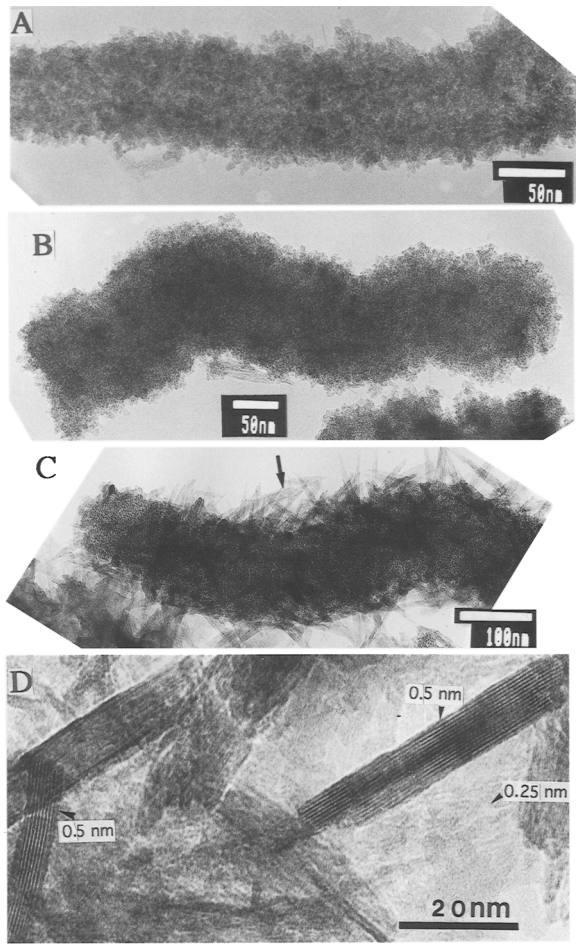

Figure 10. Transmission electron micrographs of reddish-brown bands showing fibrous bacteria with granular iron oxides (ferrihydrite; A, B) and well-crystallized spinal goethite with 0.5-nm lattice images on the cell wall (C, D).

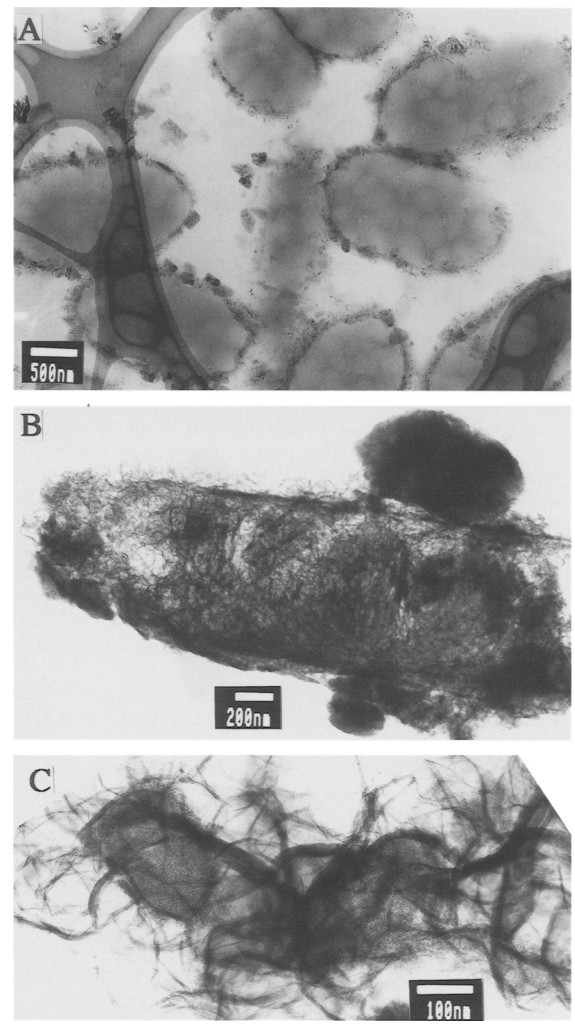

Figure 11. Transmission electron micrographs of a dark Mn-rich band showing coccus bacteria with low-density cubic minerals (A) and fine spines and long bundles of hair-like manganese oxides on the cell wall (B, C).

1992; Fortin *et al.,* 1998). The processes of iron and manganese mineralization in these deep-sea environments show that zebra architecture can be formed under intermittent oxidizing and reducing conditions (Henisch, 1988; Tazaki, 1995; Tazaki *et al.,* 1995; Tazaki and Ishida, 1996; Lovley, 1997). However, the present iron-manganese banded structures at Satsuma-Iwo Jima are being produced under aerobic conditions in a warm shallow-water environment. Thus, they represent a new type of zebra architecture which is produced solely under aerobic conditions.

ACKNOWLEDGMENTS

My thanks to K. Tawara. H. Shikaura, and H. Watanabe of Kanazawa University for their technical assistance, and to B. Roser and P. Murrow of Shimane University for review of an early draft of the manuscript. This study was partially supported by a Grant-in-Aid for Scientific Research from the Ministry of Education, Science and Culture, Japan (Grant-in-Aid for Scientific Research B).

REFERENCES

Brown, D.A., Sawicki, J.A., and Sherriff, B.L. (1998) Alteration of microbially precipitated iron oxides and hydroxides. *American Mineralogist,* **83,** 1419–1425.

Brown, D.A., Sherriff, B.L., Sawickl, J.A., and Sparling, R. (1999) Precipitation of iron minerals by a natural microbial consortium. *Geochimica et Cosmochimica Acta,* **63,** 2163–2169.

Costerton, J.W., Lewandowski, Z., and Korber, R. (1995) Microbial biofilms. *Annual Review, Microbiology,* **49,** 711.

Emerson, D. and Revsbech, N.P. (1994) Investigation of an iron-oxidizing microbial mat community located near Aarhus, Denmark: Field studies. *Applied Environmental Microbiology,* **60,** 4022–4031.

Ferris, F.G., Fyfe, W.S., and Beveridge, T.J. (1987) Manganese oxide deposition in a hot spring microbial mat. *Geomicrobiology Journal,* **5,** 33–41.

Fortin, D., Ferris, F.G., and Scott, S.D. (1998) Formation of Fe-silicates and Fe-oxides on bacterial surfaces in samples collected near hydrothermal vents on the Southern Explorer

Ridge in the northeast Pacific Ocean. *American Mineralogist,* **83,** 1399–1408.

Frankel, R.B. and Blakemore, R.P. (1991) *Iron Biominerals.* Plenum Publisher, New York, 434 pp.

Hannington, M.D. and Jonasson, I.R. (1992) Fe and Mn oxides at seafloor hydrothermal vents. In *Biomineralization Processes of Iron and Manganese—Modern and Ancient Environments,* H.G. Skinner and R.W. Fitzpatrick, eds., Catena, Cremlingen, Germany, 351–370.

Henisch, H.K. (1988) *Crystals in Gels and Liesegang Rings.* Cambridge University Press, Cambridge, 197–220.

Holden, C. (1998) Nature's art. *Science,* **282,** 1983.

Lawrence, J.R., Korber, D.R., and Caldwell, D.E. (1991) Optical sectioning of microbial biofilms. *Journal of Bacterialogy,* **173,** 6558–6567.

Lovley, D.R. (1997) Microbial Fe(III) reduction in subsurface environments. *FEMS Microbiology Reviews,* **20,** 305–313.

Mandernack, K.W., Post., J., and Tebo, B.M. (1995) Manganese mineral formation by bacterial spores of marine bacillus, strain SG-1: Evidence for the direct oxidation of Mn(II) to Mn(IV). *Geochimica et Cosmochimica Acta,* **59,** 4393–4408.

Nealson, K.H. and Stahl, D.A. (1997) Microorganisms and biogeochemical cycles: What can we learn from layered microbial communities? In *Geomicrobiology: Interactions Between Microbes and Minerals,* J.F. Banfield and K.H. Nealson, eds., Mineralogical Society of America, Washington, D.C., 5–34.

Ono, K., Soya, R., and Hosono, T. (1982) *Geology of Satsuma-Iou Jima District.* Geological Survey of Japan, Tsukuba, 45–64.

Reitner, J. and Neuweiler, F. (1995) Mud mounds: A polygenetic spectrum of fine-grained carbonate buildups. *FACIES,* **32,** 1–70.

Skinner, H.G. and Fitzpatrick, R.W., eds. (1992) *Biomineralization Processes of Iron and Manganese—Modern and Ancient Environments.* Catena, Cremlinger, Germany, 432 pp.

Tazaki, K. (1995) Electron microscopic observation of biomineralization in biomats from hot springs. *Journal of the Geological Society of Japan,* **101,** 304–314.

Tazaki, K. (1997) Biomineralization of layer silicates and hydrated Fe/Mn oxides in microbial mats: An electron microscopical study. *Clays and Clay Minerals,* **45,** 203–212.

Tazaki, K. (1999) Architecture of biomats reveals history of geo-, aqua-, and bio-systems. *Episodes,* **22,** 21–25.

Tazaki K. and Ishida, H. (1996) Bacteria as nucleation sites for authigenic minerals. *Journal of the Geological Society of Japan,* **102,** 866–878.

Tazaki, K., Ishida, H., and Fyfe, W.S. (1995) Calcite deposition in hot spring microbial mat from Iceland. In *Proceedings of the International Clay Congress,* G.J. Churchman, R.W. Fitzpatrick, and R.A. Eggleton, eds., Adelaide, Australia, 30–37.

Tazaki, K., Aoki, A., Asada, R., and Yamamura, T. (1998) A new world in the science of biomineralization: Environmental biomineralization in microbial mats in Japan. *Science Report Kanazawa University,* **XLII,** 1–65.

Tebo, B.M., Ghiorse, W.C., van Waasbergen, L.G., Siering, P.L., and Caspi, R. (1997) Bacterially mediated mineral formation: Insights into manganese (II) oxidation from molecular genetic and biochemical studies. In *Geomicrobiology: Interactions Between Microbes and Minerals,* J.F. Banfield and K.H. Nealson, eds., Mineralogical Society of America, Washington, D.C., 5–34.

Yoshizu, K. and Tazaki, K. (1997) Role of microorganisms in iron and manganese mineral formation. *Mineralogical Journal of Japan,* **26,** 69–72.

E-mail of corresponding author: kazuet@kenroku.kanazawa-u.ac.jp

(Received 28 October 1999; accepted 23 April 2000; Ms. 389; A.E. William F. Jaynes)